# Low-energy differential cross sections of pion-proton ($\pi^{\pm}p$) scattering. I. The isospin-even forward scattering amplitude at $T_\pi = 32.2$ and 44.6 MeV

Ch. Joram,* M. Metzler,† J. Jaki,‡ W. Kluge, H. Matthäy,§ and R. Wieser
*Institut für Experimentelle Kernphysik, Universität Karlsruhe, Postfach 3640, D-76021 Karlsruhe, Germany*

B. M. Barnett,‖ H. Clement, S. Krell,¶ and G. J. Wagner
*Physikalisches Institut, Universität Tübingen, Auf der Morgenstelle 12, D-72076 Tübingen, Germany*
(Received 8 November 1994)

The values of the pion nucleon ($\pi N$) $\sigma$ term, as determined, on the one hand, from experimental pion nucleon scattering by means of dispersion relations and, on the other hand, from baryon masses by means of chiral perturbation theory, differ by 10 to 15 MeV. The origin of this discrepancy is not yet understood. If the difference between the two values is attributed to the scalar current of strange sea quark pairs within the proton, the contribution to the proton mass would be of the order of 120 MeV. The discrepancy may hint at either theoretical deficiencies or an inadequate $\pi N$ database. In order to provide reliable experimental data we have measured angular distributions of elastic pion proton scattering at pion energies $T_\pi = 32.2$ and 44.6 MeV using the magnet spectrometer LEPS located at the Paul-Scherrer-Institute (PSI) in Villigen, Switzerland. From the data covering the region of the Coulomb nuclear interference, the real parts of the isospin-even forward scattering amplitude $\mathrm{Re}D^+(t=0)$, have been determined as a function of energy. The results have been compared with the predictions of the Karlsruhe-Helsinki phase shift analysis KH80, revealing discrepancies most pronounced for the $\pi^+p$ data. The experimentally determined values for $\mathrm{Re}D^+(t=0)$, however, support the KH80 prediction (which is based on $\pi N$ data available in 1979).

PACS number(s): 13.75.Gx, 21.45.+v, 25.80.Dj

## I. INTRODUCTION

The pion nucleon $\sigma$ term, which is a measure of the explicit chiral symmetry breaking of QCD, has attracted great attention during recent years [1–3]. A reason for that is that the $\sigma$ term might provide evidence for the existence of strange sea quark pairs in the nucleon, at small four-momentum transfer. Strange sea quark pairs seem to contribute to static properties of the nucleon, to its mass [2–6], spin [7–9], and magnetic moment [10–14].

The $\sigma$ term quantifying the explicit breaking of the chiral symmetry of QCD by the quark masses can be calculated, on the one hand, within the framework of chiral perturbation theory ($\chi$PT) of low-energy QCD from baryon masses. Gasser and co-workers calculated the $\sigma$ term [2–6] in one-loop approximation of $\chi$PT:

$$\sigma_{\pi N}(0,0) = \frac{35 \pm 5\ \mathrm{MeV}}{1-y} \quad \text{where } y = \frac{2\langle p|\bar{s}s|p\rangle}{\langle p|\bar{u}u+\bar{d}d|p\rangle}\,. \quad (1)$$

The parameter $y$ describes possible contributions of strange sea quarks to the $\sigma$ term, i.e., to the mass of the nucleon. On the other hand, the $\sigma$ term is related by a low-energy theorem (see Ref. [5]) to the isospin-even pion nucleon amplitude $\Sigma_{\pi N}$ at the unphysical Cheng-Dashen point $\nu = (s-u)/4m_N = 0$ and $t = 2m_\pi^2 = 2\mu^2$:

$$\Sigma_{\pi N}(0,2m_\pi^2) = -f_\pi^2 \bar{D}^+(0,2\mu^2) = \sigma_{\pi N}(0,0) + \Delta_\sigma + \Delta_R\,. \quad (2)$$

Here $\bar{D}^+$ denotes the forward scattering amplitude from which the pseudovector Born term $g_{\pi NN}^2/m_N$ has been subtracted. The pion decay constant $f_\pi$ has the numerical value 92.4 MeV [15]. The term $\Delta_\sigma$ is given by the difference of the scalar form factors at $\nu = 2\mu^2$ and $\nu = 0$, $\Delta_\sigma = \sigma(0,2\mu^2) - \sigma(0,0)$, and $\Delta_R$ is a higher-order correction to $\Delta_\sigma$ which is given below.

The amplitude $\Sigma_{\pi N}(0,2\mu^2)$ at the unphysical Cheng-Dashen point can also be evaluated from $\pi N$ scattering amplitudes determined experimentally for $t \leq 0$. This program of analytical continuation from the physical region to the Cheng-Dashen point using dispersion relations has been performed by the Karlsruhe-Helsinki (KH) group [16]. Koch and Pietarinen [17] carried out a phase shift analysis (KH80) which extends to low energies and respects analyticity and unitarity and conse-

*Now at CERN, PPE Division, CH-1211 Genève 23, Switzerland.
†Now at Gesellschaft für Elektronische Informationsverarbeitung, D-64283 Darmstadt, Germany.
‡Now at Pietzsch AG, Automatisierungstechnik, Hertzstr. 32, D-76275 Ettlingen, Germany.
§Now at Institut für Experimentalphysik I, Ruhruniversität, Bochum, Postfach 10248, D-44801 Bochum, Germany.
‖Now at Institut für Strahlen- und Kernphysik der Universität Bonn, Nußallee 14-16, D-53115 Bonn, Germany c/o CERN, PPE Division, CH-1211 Genève 23, Switzerland.
¶Now at Temic Telefunken Microelectronics, Sieboldstr. 19, D-90411 Nürnberg, Germany.

 ©1995 The American Physical Society

quently allows a unique extrapolation both to the $\pi N$ threshold (to determine the scattering lengths) and to the Cheng-Dashen point (to determine the amplitude $\Sigma$). Koch (1982) used dispersion relations along hyperbolas in the $\nu$-$t$ plane [16]. He obtained a value of $\Sigma_{\pi N}(0, 2\mu^2) = 64 \pm 8$ MeV.

Gasser and co-workers [4–6], working on the premise that the isospin-even scattering lengths $a^+_{0+}$ and $a^+_{1+}$ for the $S_{1/2}$ and $P_{3/2}$ waves as well as the imaginary parts of certain invariant amplitudes for $k_{\rm lab} > 172$ MeV/$c$ are correctly described by the KH80 solution, obtained $\Sigma_{\pi N}(0, 2\mu^2) \approx 60$ MeV in a related dispersion analysis. This confirms the consistency of the Karlsruhe-Helsinki analysis.

Gasser, Leutwyler, and Sainio [4], also using a dispersion relation, calculated $\Delta_\sigma \approx 15$ MeV and, within the framework of chiral perturbation theory, calculated the term $\Delta_R = 0.35$ MeV [6], taking into account contributions of the order $\mu^4 \ln\mu^2$. Consequently, the relation between the $\pi N$ amplitude $\Sigma_{\pi N}(0, 2\mu^2)$ and the $\sigma$ term is, in one-loop approximation of $\chi$PT, $\Sigma_{\pi N} \approx \sigma(0,0) + 15$ MeV. Obviously the two values of $\Sigma_{\pi N}$ as obtained from the baryon mass spectrum and from $\pi N$ scattering are different:

$$\sigma_{\pi N} = \frac{35 \pm 5 \text{ MeV}}{1 - y} = 45\text{–}50 \text{ MeV and } y \approx 0.2 \pm 0.2 .$$

If the "large" value of $\Sigma_{\pi N}$ was interpreted to be the result of the existence of strange sea quark pairs in the nucleon, it had the consequence that the matrix element of the scalar density of strange quark-antiquark pairs $m_s\langle p|\bar{s}s|p\rangle$ contributed about 120 MeV to the nucleon mass [4].

Data on low-energy $\pi^\pm p$ interactions (below $\approx$ 300 MeV) are particularly important for the determination of the $\sigma$ term. The existing data [18] (see also the compilations in Refs. [19–22]) are, however, partly contradictory and inconsistent, making new measurements highly desirable. In our continuing experimental program [23,24], we have measured angular distributions of elastic pion-proton scattering at pion energies $T_\pi = 32.2$, 44.6, and 68.6 MeV. Preliminary results have been presented in Refs. [19,20,25,26].

In this paper (quoted as paper I in the following) we will describe the data taken at pion energies $T_\pi = 32.2$ and 44.6 MeV at angles between 10° and 45°, and in a second paper (paper II) we will publish the full angular distributions at the three energies and a combined analysis of all data. The reason for this two-part publication lies in the different methods used in analyzing the data. While the data in the Coulomb nuclear interference region (paper I) allow a direct determination of the real parts of the isospin-even forward scattering amplitudes $\mathrm{Re}D^+(s, t = 0)$, the full angular distributions provide the $S$- and $P$-wave phase shifts at low energies. In this paper considerable space has been devoted to the description of the experimental setup and the basic features of the analysis allowing us to cut (to a minimum) this part in paper II.

In a previous experiment we determined that $\mathrm{Re}D^+(t = 0)$ at $T_\pi = 54.3$ MeV [23,24]. $\mathrm{Re}D^+(t = 0)$ can be obtained experimentally from the difference of the measured $\pi^\pm p$ cross sections $d\sigma_\pm/d\Omega$, without any partial wave analysis, and can be compared directly with the results obtained with the dispersion analyses:

$$\mathrm{Re}D^+(\nu, t = 0) = \lim_{t\to 0} \frac{4\pi\sqrt{s}}{m_N}\Delta(t)$$

where

$$\Delta(t) = \frac{1}{4\mathrm{Re}G_C(t)}\left[\frac{d\sigma_{\pi^+p}}{d\Omega}(t) - \frac{d\sigma_{\pi^-p}}{d\Omega}(t)\right] \qquad (3)$$

with $G_C(t)$ being the pure Coulomb spin (nonflip) amplitude. As will be shown in Sec. III H, the experiment that will be described forthwith allows the determination of $\mathrm{Re}D^+(t = 0)$ in various partly independent ways.

This paper comprises a description of the experimental method (Sec. II), of the details of the data analysis, and a discussion of the results (Sec. III). The data are compared exclusively with the predictions of the Karlsruhe-Helsinki phase shift analysis of 1979/80 [17], because this analysis respects Mandelstam analyticity and unitarity.

## II. EXPERIMENTAL METHOD

### A. Principle of the experiment

The goal of the experiment is the absolute determination of the differential cross sections for $\pi^\pm p$ scattering at the energies $T_\pi = 32.2$ and 44.6 MeV:

$$\frac{d\sigma}{d\Omega}(\pi^\pm p) = \frac{N_\pi^{\rm scatt}(\theta)}{N_\pi^{\rm in} N_p^{\rm tgt} d\Omega \varepsilon_\pi} . \qquad (4)$$

This requires the determination of the following experimental quantities with the highest possible precision: the number of incident pions $N_\pi^{\rm in}$ impinging the target, the number of pions $N_\pi^{\rm scatt}(\theta)$ scattered through the angle $\theta$, the number of protons per target area, $N_p^{\rm tgt}$, the effective solid angle $d\Omega$ subtended by the detector, and the efficiency of particle detection and other corrections, $\varepsilon_\pi$.

The experiment was carried out in the $\pi$E3 channel of Paul-Scherrer-Institute (PSI) in Switzerland. Figure 1 shows, schematically, the experimental setup. The particles scattered from the target were detected in the high-resolution magnet spectrometer LEPS (low-energy pion spectrometer) [27,28]. The principle of this experiment may be described as a single-arm measurement with momentum analysis and is, to our knowledge, employed here for the first time in a low-energy $\pi^\pm p$ scattering experiment. The recoil protons emerging from the target have not been detected.

The flux of incoming particles was measured using a segmented scintillator hodoscope mounted downstream of the scattering target. In addition, a relative normalization of the pion flux has been obtained from four small scintillator telescopes positioned concentrically around the beam tube some 60 cm upstream of the scattering target. Both detector arrangements are described in detail in Ref. [29].

The effective solid angle of the spectrometer has been determined by exploiting the electromagnetic scattering

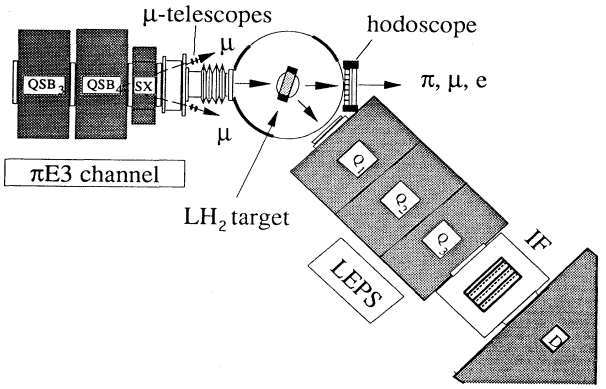


FIG. 1. Experimental setup.

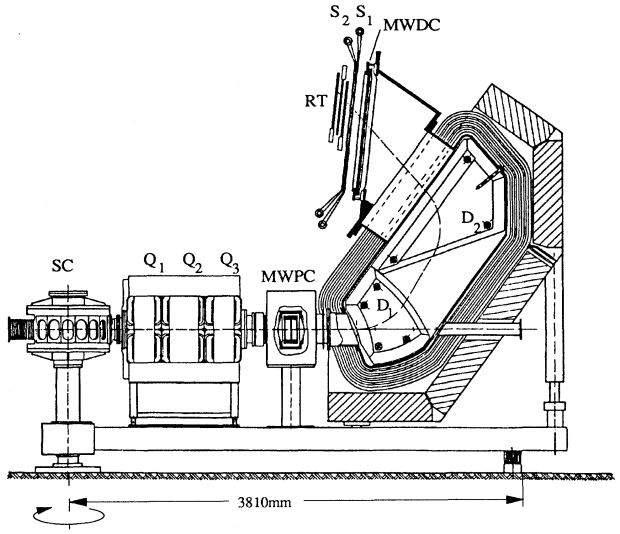


FIG. 2. Magnet spectrometer LEPS.

of muons from protons, which has been simultaneously measured in our setup. This is feasible since the cross section for this reaction, which normally affects the data as a disturbing background, can be calculated with high precision. Transforming Eq. (4) and replacing all pionic quantities by the corresponding muonic ones, results in

$$d\Omega = \frac{N_\mu^{\rm scatt}(\theta)}{N_\mu^{\rm in} N_p^{\rm tgt} [d\sigma(\mu^\pm p)/d\Omega] \varepsilon_\mu} \,. \tag{5}$$

After replacing $N_\mu^{\rm in}$ and $N_\pi^{\rm in}$ by $N^{\rm in} R_\mu$ and $N^{\rm in} R_\pi$, respectively, with $R_\pi$ and $R_\mu$ being the relative fractions of pions and muons in the incident beam, Eq. (5) may be inserted into Eq. (4):

$$\frac{d\sigma}{d\Omega}(\pi^\pm p) = \frac{N_\pi^{\rm scatt}(\theta)}{N_\mu^{\rm scatt}(\theta)} \frac{R_\mu}{R_\pi} \frac{\varepsilon_\mu}{\varepsilon_\pi} \frac{d\sigma}{d\Omega}(\mu^\pm p) \,. \tag{6}$$

Obviously the number of target protons as well as the absolute incident flux cancel in this approach.

The cross sections at scattering angles ranging from 10° to 45° in the laboratory system have been measured using a 40 mm thick liquid hydrogen ($LH_2$) target. Measurements with the target cell empty have been carried out to allow the subtraction of background. The measurement of the particle momentum allows the distinction between particles scattered from protons and those scattered from other nuclei by means of the reaction kinematics alone.

In the following we describe the experimental setup in more detail, including the pion channel and the spectrometer with the attached detectors, as well as the liquid hydrogen target. Subsequently the data acquisition, absolute momentum calibration, and the experimental procedure will be discussed.

### B. The magnet spectrometer LEPS at the πE3 channel of PSI

The low-energy pion spectrometer LEPS consists of two dipole magnets in a split pole configuration and a symmetric triplet of quadrupole magnets placed in front of the dipoles (see Fig. 2). The triplet forms an image of the scattered beam at the target in the intermediate focus (IF). In the intermediate focus a multiwire proportional chamber composed of three $x$ and three $y$ readout planes allows the measurement of the coordinates $x_{\rm IF}$ and $y_{\rm IF}$, as well as the angles $\theta_{\rm IF}$ and $\phi_{\rm IF}$. The focal plane of the split pole magnet is tilted by 43° with respect to the central trajectory. This permits the use of a vertical drift chamber to determine the coordinate $x_{\rm FP}$ and the angle $\theta_{\rm FP}$ in the focal plane. The most important features of these detectors are summarized in Table I. An arrangement of scintillation detectors is placed downstream of the drift chamber. The detectors are used as trigger counters (scintillators S1 and S2), and as a range telescope (scintillators R1, R2, and R3).

LEPS can be rotated around the center of the scattering chamber to angles in the range from −5° to 123°. For experiments with LEPS, the low-energy pion channel πE3 of PSI is operated in a chromatic mode which provides a vertical dispersion (in the $x$ direction) at the scattering target (ST) of $D_{\rm ST} = -5$ cm/%. The size of the beam spot at the scattering target is $\Delta x_{\rm ST} = \pm 5$ cm and $\Delta y_{\rm ST} = \pm 2$ cm, respectively, resulting in a momentum band of $\Delta p/p = \pm 1\%$. The momentum resolution of the channel is about 0.5% full width at half maximum (FWHM). The divergences at the scattering target are $\Delta\theta = 35$ mrad and $\Delta\phi = 80$ mrad (FWHM). The divergence in the horizontal plane $\Delta\phi$ limits the precision of the determination of the scattering angle. The channel, consisting of three dipole, ten quadrupole, and one sextupole magnets, has a total length of about 15 m. Both flux and beam spot size at the target can be adjusted by a system of slits. Typical pion rates are $5 \times 10^6$ s$^{-1}$ for positive and $1 \times 10^6$ s$^{-1}$ for negative polarity, respectively.

The momentum of the incident particles is measured by the spectrometer itself, exploiting the chromaticity of the beam which relates the momentum of the particles to their $x$ coordinate $x_{\rm ST}$ at the scattering target. This coordinate is determined by tracing back the particles using the coordinates measured at the IF of LEPS, and

TABLE I. Multiwire detectors of LEPS.

| | Intermediate focus | Focal plane |
|---|---|---|
| Type of chamber | MWPC with 6 readout planes | Vertical drift chamber |
| Number of sense wires | $6 \times 128$, 1 mm pitch | 240, 4 mm pitch |
| Diameter of sense wires | 10 $\mu$m | 20 $\mu$m |
| Diameter of field wires | | 45 $\mu$m |
| Gap width | 5 mm | 10 mm |
| Counting gas | 79.2% argon, 20% isobutane, 0.8% freon | 50% argon, 50% isobutane |
| High voltage | 4.7 kV | 7.2 kV |
| $\sigma_x$ | 360 $\mu$m | 310 $\mu$m |
| $\sigma_\theta$ | 5.6 mrad | 6 mrad |
| $\sigma_y$ | 360 $\mu$m | not measured |
| $\sigma_\phi$ | 6.8 mrad | not measured |

taking advantage of the precisely known ion optics of the quadrupole triplet.

The momentum of the scattered particles is measured in the focal plane of LEPS by means of the vertical drift chamber (the dispersion being $D = 2$ cm/%). Second- and higher-order effects such as chromatic aberrations are also compensated by employing the coordinates and angles measured in the IF. The resulting momentum resolution $\delta p/p_{\mathrm{LEPS}}$ is better than 0.2% (FWHM).

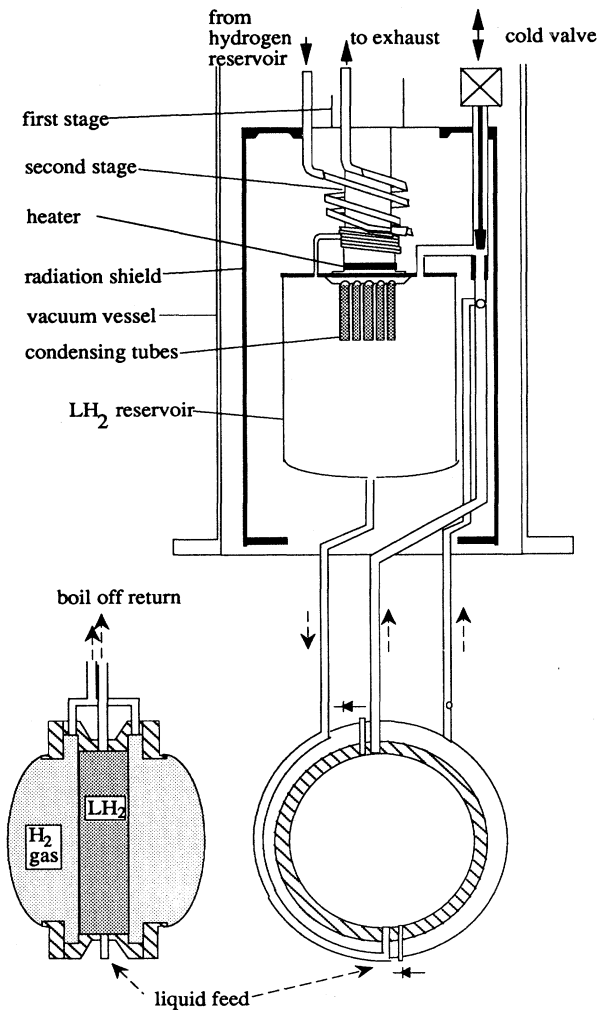


FIG. 3. The liquid hydrogen target.

### C. The liquid hydrogen target

The measurements (in the Coulomb nuclear interference region) have been carried out using a 40 mm thick cylindrical liquid hydrogen target, placed with its axis along the scattering plane. It consists of a stainless steel cell with a diameter of 150 mm. As shown in Fig. 3, an inner target cell which is filled with liquid hydrogen is separated from the two outer cells, filled with cold hydrogen gas, by 30 $\mu$m thick Mylar foils. The outer cells are covered by 160 $\mu$m thick Mylar foils. All three cells are connected in order to maintain the same vapor pressure. The thin windows of the cell with liquid hydrogen were prestretched at a temperature of 120 °C prior to assembling the target. As a consequence, bulging of these foils due to the hydrostatic pressure of the $LH_2$ is negligible. A small meshed container filled with active carbon and placed at the bottom of the inner cell catalyzes the transition of orthohydrogen to parahydrogen, the densities of which are slightly different.

The target and the two-step refrigerator, with a power of 34 W at 80 K and 10 W at 20 K, form a closed system. The net power of the second step of the liquifier can be adjusted by means of a heating coil surrounding it. This ensures that a constant value for the vapor pressure inside the target, and consequently for the density of the liquid hydrogen, is maintained: $p = 1050 \pm 5$ hPa, $r = (70.0 \pm 0.025) \times 10^{-3}$ g/cm$^3$. The level of the liquid in the target cells was monitored by two temperature sensitive diodes, one at the bottom and the other at the top of the inner cell. The refrigerator system being equipped with a 1.5 l reservoir for liquid hydrogen, allowed the emptying or refilling of the target cell within a few minutes by means of a so-called cold valve. For more details of the liquid target, see Ref. [23].

### D. Data acquisition

The main components of the data acquisition are shown schematically in Fig. 4. The boxes in the upper

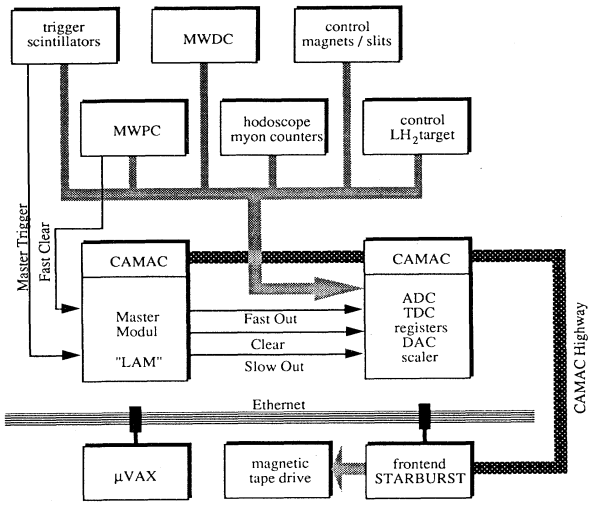


FIG. 4. Schematic drawing of the main components of the data acquisition system.

part of the figure symbolize the various sources of information: detectors, control units for magnets and slit systems, and the $LH_2$ target. The electronic modules (ADC, DAC, TDC, registers, scalers), housed in CAMAC crates, are shown below. These modules are read out by a front-end computer which writes the data to tape. A $\mu$VAX connected to the front-end via ethernet is used to control the complete system and to perform an on-line analysis of part of the data.

The so called "master module," also housed in a CAMAC crate, is of great importance in the two-step trigger decision. About 40 ns after a particle has crossed the trigger scintillators in the focal plane of LEPS the master trigger (MT) signal is fed to the master module. If the processing of the preceding event has been completed, the fast out (FO) signal is generated by the master module within 20 ns. This signal is used to stop the TDC modules of the multiwire drift chamber (MWDC) and to gate the registration of hits in the multiwire proportional chamber (MWPC) electronics. The input of the master module is then locked for forthcoming master triggers. The ratio of the counting rates $\varepsilon_{\text{comp}}$ =FO/MT is a measure of the dead time of the data acquisition system, and has to be taken into account during the data analysis. Some 400 ns after the FO, the master module checks for an occurrence of the fast clear signal, which will have been generated by a MWPC logic if less than two $x$ and two $y$ planes have fired. If such a signal is not available, the master module sends a LAM signal to the front-end computer initiating the read-out of all CAMAC modules. Otherwise the content of all modules is cleared. Subsequent to the fast clear or the completion of the acquisition phase, the lock of the master module is removed so that the system is ready to accept new events.

### E. Momentum calibration of the incident pion beam

Great attention has been paid to the precise calibration of the momentum of the incident beam. Three difference methods have been employed: (a) time-of-flight (TOF) measurements of pions with respect to the radio-frequency (rf) signal of the isochronous cyclotron, (b) TOF measurements for protons, and (c) energy measurements by the stopping of protons and deuterons emitted from the pion production target in a silicon surface barrier detector.

Methods (a) and (b) take advantage of the time structure of the beam introduced by the rf period $T_{\text{cycl}}$ of the cyclotron (precisely 19.75 ns). At first the TOF with respect to the rf is measured with a scintillation counter at a position $z_1$. Then the counter is moved downstream to a position $z_2$ where the distance $z = z_2 - z_1$ is chosen exactly, such that the measured TOF of the particles (pions or protons) is the same, modulo 19.75 ns. The velocity of the particles is then $\beta c = z/T_{\text{cycl}}$. Neither electronic nonlinearities nor any calibration of the TDC have influence on the precision of this method. The error in the velocity is driven only by the uncertainties with which the equality of the TOF measurements and the distance $z$ can be determined:

$$c\Delta\beta = \left|\frac{1}{T_{\text{cycl}}}\Delta z\right| + \left|\frac{\beta c}{T_{\text{cycl}}}\Delta t\right| . \tag{7}$$

The error of the time measurement is $\Delta t = \pm 25$ ps. Typical values for $z$, are about 4 and 0.7 m for pions and protons, respectively. The uncertainty of the distance for pions is about $\Delta z = \pm 1$ cm. Taking into account the corrections for energy losses in foils and air and the corresponding errors, the error for the pion momentum is found to be about $\Delta p = \pm 1$ MeV/$c$:

$$\Delta p = \frac{dp}{d\beta}\Delta\beta = p\left(\frac{1}{\beta} + \beta\gamma^2\right)\Delta\beta . \tag{8}$$

The measurements for protons have been performed in vacuum. The scintillation counter inside the vacuum vessel has been mounted on a sliding carriage being moved by means of a threaded bar. The position of the scintillator has been derived from the number of rotations of the bar with an uncertainty of $\pm 0.5$ mm. The precision of this position measurement, combined with the low $\beta$ for protons, leads to a smaller error for this method: $\Delta p = \pm 0.3$ MeV/$c$.

Method (c) turns out to give results which were systematically lower than those obtained with the methods (a) and (b). The explanation could be found in the energy calibration of the silicon surface barrier (SSB) detector, which is usually achieved by using alpha particles from various sources with energies $5 < E_\alpha < 9$ MeV. In our case an $^{241}$Am source ($E_\alpha = 5.482$ MeV) and a

TABLE II. Momentum and energy of incident pions at the center of the scattering target.

| | $p_\pi$ (MeV/$c$) | $E_\pi$ (MeV) | $p_\pi$ (MeV/$c$) | $E_\pi$ (MeV) |
|---|---|---|---|---|
| (a) TOF of pions | $100.9 \pm 1.0$ | $32.6 \pm 0.51$ | $119.3 \pm 1.1$ | $44.0 \pm 0.7$ |
| (b) TOF of protons | $100.15 \pm 0.3$ | $32.2 \pm 0.17$ | $120.2 \pm 0.3$ | $44.6 \pm 0.2$ |

$^{212}$Po/$^{212}$Bi source[1] ($E_\alpha$ = 8.780 and 6.049 MeV) were used to calibrate the SSB detector simultaneously with protons and deuteron measurements to avoid rate dependent effects in the detector and in the electronic circuits. The relation between the pulse height $h^{\text{pulse}}$ of the detector signal and the deposited energy $E$, however, does contain terms dependent on the projectile mass and can generally be expressed by

$$h^{\text{pulse}} = [a + a'(m, E)] + [b + b'(m, E)]E\,.$$

Unless all coefficients (in particular $a'$ and $b'$) which can vary slightly with the deposited energy are precisely known, a SSB detector being calibrated with $\alpha$ particles may give incorrect results for different types of particles, especially if the measurements are performed in different energy ranges. For proton and deuteron measurements the deviation may be of the order of 1–2 %, as has been described in the literature [30]. Therefore we conclude that method (c) is not appropriate for use in the calibration of a low-energy pion beamline to the required precision. The results for the pion momenta at the center of the target as determined by methods (a) and (b) are given in Table II. Due to their superior accuracy, the momenta determined with method (b) are taken as the reference values in the following.

### F. Experimental procedure

The measurements covered the angular range from 10° to 45° in steps of 5°. The 40 mm thick $LH_2$ target, being placed in the evacuated scattering chamber, was pivoted for all runs at 15° with respect to the incident beam. Due to a large window in the chamber, all scattering angles could be investigated without breaking the vacuum. The central momentum of LEPS, $p_0$, was adjusted for each measurement in order to correct for the energy difference of measurements with full and empty target as well as for the energy loss due to the recoil of the protons. Consequently, pions scattered from protons were always detected with the same relative momentum, $\delta = (p - p_0)/p_0$. In this way, the dependence of the spectrometer solid angle on the relative momentum implies that only very minor corrections need to be made in the analysis. Great care has been taken in precisely reproducing the strength of the magnet fields, for both LEPS and the beamline. The currents of the magnets have been set following a fixed cycle to minimize hysteresis effects.

[1]The $^{212}$Po/$^{212}$Bi source was produced just before the measurements in a dedicated setup. Starting with a small quantity of $^{232}$U in a closed box, volatile $^{220}$Rn is produced in the natural decay sequence. The atoms arising in the subsequent decays of $^{220}$Rn are ionized due to the recoil and can easily be deposited onto a thin aluminum foil by applying a voltage of some 250 V. At the end of this decay sequence, $\alpha$ particles from the decays of $^{212}$Bi and $^{212}$Po with energies $E_\alpha$ = 6.049 and 8.780 MeV are observed. The half-life of the source is governed by the isotope with the longest half-life in the decay sequence, namely, $^{212}$Pb ($T_{1/2}$ = 10.6 h).

## III. DATA ANALYSIS

### A. Overview

As outlined in Sec. II, our experimental method does not require any calibration of the absolute flux of the particles hitting the target. To identify incident particles and to determine the relative numbers of pions and muons, their time of flight with respect to the cyclotron rf signal has been measured in the scintillator hodoscope. A relative measure of the incident flux, which is indispensable in the normalization of runs with full and empty target cells to the same number of incident pions or muons, is provided by the four muon telescopes (see Fig. 1).

Scattered particles are identified using TOF information from the trigger scintillators in the focal plane of LEPS. To resolve ambiguities due to the relatively short period of the rf signal (19.75 ns), $dE/dx$ and range information has been exploited. Muons originating from pion decays in the dipoles of LEPS are identified by tracing their trajectory, as determined from measurements of coordinates and angles at the intermediate focus and in the focal plane. The steep angular dependence of the cross sections for both pion and muon scattering, together with the large angular acceptance of LEPS ($\Delta\theta \leq 5°$), give rise to corrections dependent on the scattering angle and the polarity of the particles. These, however, could be limited to values below 10% by splitting up the angular acceptance of LEPS into intervals of $\Delta\theta = 1°$ and by restricting the analysis to events with $\Delta\theta \leq 3°$.

The precise determination of $\text{Re}D^+(\nu, t = 0)$ was one of the main motivations for this experiment. As will be shown below, this quantity can be related not only to the difference of the differential cross sections for $\pi^+ p$ and $\pi^- p$ scattering, but also to the ratio of the two. Therefore a second independent analysis focused on the accurate fixing of this ratio. The advantage of this approach is found in a reduction of systematic errors.

### B. Particle identification in the incident beam

The relative fractions of pions, muons, and electrons in the incident beam are measured by their TOF relative to the rf signal of the cyclotron in a hodoscope which has been placed 45 cm downstream of the scattering target. A detailed description of the scintillator hodoscope

can be found in Ref. [29]. The TOF measurements imply that times can be determined only modulo the rf period (19.75 ns), which in turn introduces partial time overlaps of pions, muons, and electrons and momentum dependent changes in the order of their arrival times. The TDC modules are sampled at the reduced rate of about 20 kHz. The information which has been stored in fast histogramming memory modules is read out at intervals of 10 min. TOF spectra for both particle charges and energies are shown in Fig. 5. The analysis of these spectra is facilitated by exploiting the proportionality of the pion and muon fraction which is practically independent of the charge of the particles. Subtracting two properly normalized TOF spectra of opposite polarity leaves the isolated electron distribution, which can then be subtracted from the original spectra. The resulting pure pion and muon peaks are well separated. The beam composition can then be determined by fitting procedures. Two aspects have to be considered with great care. First, muons originating from pion decays upstream of the hodoscope contribute to a "bridge" between the pions and muons which also extends under the pion peak. Secondly, the composition measured with the hodoscope has to be corrected for pion decays between the scattering target and the hodoscope. Detailed studies with the code DECAY TURTLE [31] predict a cancellation of these two effects to better than 1%, at the energies of our experiment. The composition of the incident beam at the scattering target has been summarized in Table III.

The four "muon telescopes" mounted concentrically outside the beam pipe detect muons originating from pion decays some 60 cm upstream. Their counting rate, being of the order of a few kHz, is therefore proportional to the number of incident pions, $N_\pi^{\rm in} = \alpha\mu_\Sigma$ where $\mu_\Sigma$ denotes the sum of the four telescopes. $\alpha$ is a constant the energy dependence of which need not be explicitly known. A relative measure for the incident muon flux is given by $N_\mu^{\rm in} = \alpha\mu_\Sigma R_\mu/R_\pi$. These relative pion and muon fluxes have been used to normalize the runs corresponding to full and empty targets to the same number of incident particles. By using the muon telescopes instead of the hodoscope, systematic errors of the absolute counting rates of the order of $10^6$ s$^{-1}$, introduced by electronic dead time and multiple particle hits from a single burst, are circumvented. In addition, ratios of the counting rates of the individual muon telescopes provide an even more sensitive monitoring of fluctuations in the beam spot than the profiles obtained with the hodoscope.

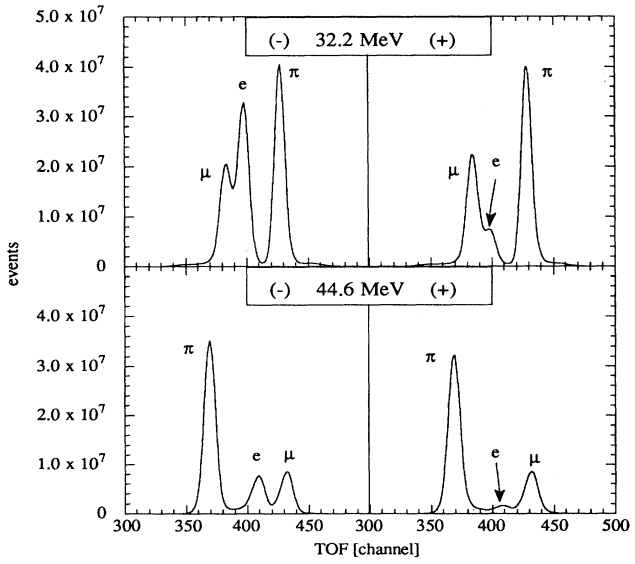


FIG. 5. Time-of-flight spectra taken with the hodoscope in the incident beam for both particle charges. 1 channel corresponds to 156 ps.

TABLE III. Composition of the incident beam at the scattering target. The statistical errors of these numbers are negligibly low. The systematic errors depend on the separation of the TOF peaks of the pions, muons, and electrons and do not exceed ±2%.

| $T_\pi$ (MeV) | Polarity | $R_\pi$ | $R_\mu$ | $R_e$ | $R_\mu/R_\pi$ |
|---|---|---|---|---|---|
| 32.2 | + | 0.524 | 0.316 | 0.102 | 0.603 |
| 32.2 | − | 0.367 | 0.222 | 0.371 | 0.605 |
| 44.6 | + | 0.685 | 0.212 | 0.057 | 0.310 |
| 44.6 | − | 0.555 | 0.164 | 0.215 | 0.296 |

### C. Identification of scattered particles

The particle identification in the scattered beam aims at the unambiguous discrimination of elastic $\pi^\pm p$ and $\mu^\pm p$ events against all sources of background. The main contribution to the background is due to the decay of pions. The effects of muon decay in the region around the scattering target and inside the spectrometer are almost negligible. Electrons scattered from protons are, however, observed as well. The relative contributions of these processes vary significantly with the scattering angle.

Most of the background arising from decays as well as the elastically scattered electrons can be removed easily by TOF measurement in the focal plane of LEPS. The path length through the spectrometer depends on the angles and relative momenta of the particles with respect to the central trajectory. However, through a precise awareness of the trajectory for each particle, determined by the various wire chambers in LEPS, we are able to correct the time of flight for different path lengths. The resulting TOF resolution of about 1 ns (FWHM) is limited finally by the time resolution of the pion channel. Two time-of-flight spectra taken at $T_\pi = 32.2$ MeV at scattering angles of 20° and 45°, respectively, are shown in Fig. 6.

At $T_\pi = 44.6$ MeV (corresponding to 120.2 MeV/$c$) a quantitative separation of muons and electrons is difficult due to partial overlaps in the TOF spectra arising from the time structure of the primary proton beam. Here the energy deposited in the trigger counters as well as the path length in the range telescope provide additional information. The energy deposit in the trigger scintillators is derived from the pulse heights of the photomultipliers which are mounted at both ends of the counters. Calcu-

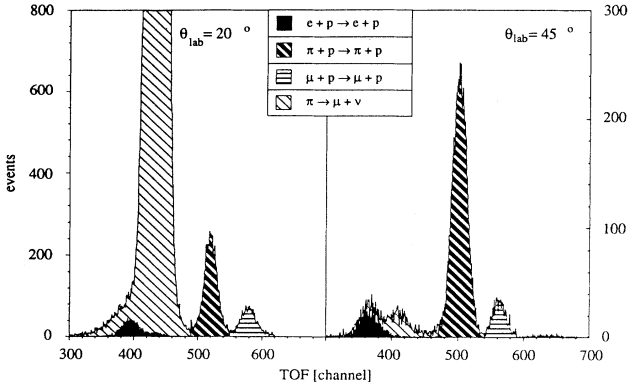


FIG. 6. Time-of-flight spectra taken at $T_\pi = 32.2$ MeV and at scattering angles $\theta_{\rm lab} = 20°$ and 45°, respectively, with the scintillation counters in the focal plane of LEPS. As explained in the text the various contributions to the spectra have been identified by means of $dE/dx$ and range measurements. 1 channel corresponds to 50 ps.

lating the geometric mean and correcting for the angular dependence of the path length, $\bar{Q}_1 = \sqrt{Q_1 Q_1'}\cos\theta$, leads to a satisfying separation of pions, muons, and electrons (see Fig. 7). The range telescope can be used to identify electrons in the focal plane. In contrast to pions and muons, electrons of the considered momentum ($\approx$ 120 MeV/$c$) do not stop in the telescope. Polyethylene absorbers of the proper thickness are positioned between the scintillators which reliably stop pions and muons in front of the last counter, $R3$. In this way, pions and muons are distinguished from electrons. A quantitative separation of pions and muons by this method alone is, however, not possible. A typical stop distribution is shown in Fig. 8.

For muons originating from pion decays in the split pole of LEPS, the remaining path length to the trigger counters is not sufficient for a clear separation by TOF. These muons are efficiently removed by checking whether

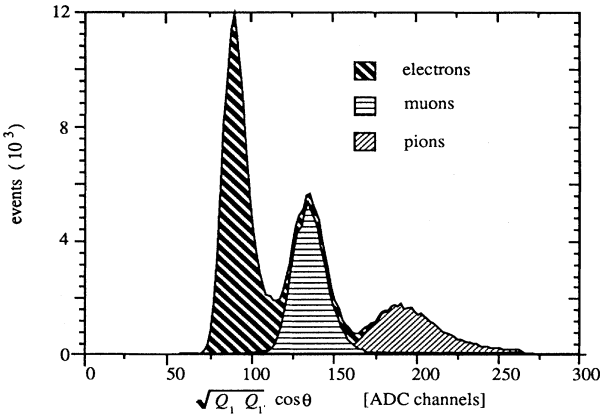


FIG. 7. Energy loss spectrum measured in trigger counter $S_1$ at $p = 120.2$ MeV/$c$ with LEPS positioned at $\theta_{\rm lab} = 0°$. The identification of the different particles has been achieved by TOF measurements.

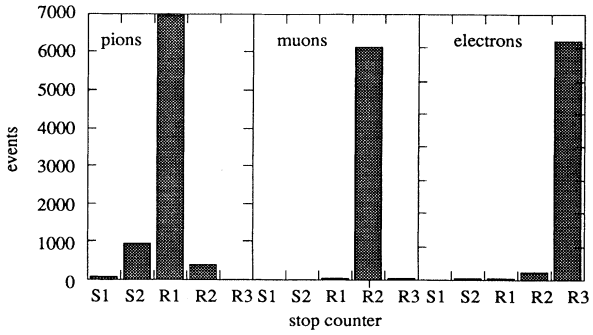


FIG. 8. Range distributions of pions, muons, and electrons at $p = 120.2$ MeV/$c$.

the radial angles measured at the intermediate focus and the final plane of LEPS are consistent with the trajectory of a nondecaying ("stable") particle. Detailed experimental studies as well as simulations with an extended version of DECAY TURTLE have proven the remaining background to be less than 1% [32].

The number of pions detected in the focal plane of LEPS must be corrected for decay losses. This is done by weighting each detected pion with a factor

$$K = \exp\left(\frac{l_{\rm path} m_\pi}{c\tau_\pi p_f}\right) . \tag{9}$$

The path length $l_{\rm path}$ from the scattering target to the focal plane as well as the momentum $p_f$ after scattering are known with good precision. Therefore although this correction is of the order of a factor of 2, it does not introduce a sizable uncertainty.

### D. Subtraction of the empty target measurements

After applying the cuts discussed in Sec. III C there remains only background from the scattering of pions and muons on the Mylar windows (chemical composition $C_5H_4O_2$) of the target. The momentum resolution, being worsened by energy straggling in the 20 mm thick hydrogen target and various vacuum windows, does not allow us to distinguish between the scattering on carbon and oxygen nuclei merely by means of the different kinematical energy transfer alone. Empty target measurements are necessary. They have been normalized to the same number of incident pions or muons by exploiting the summed counting rates $\mu_\Sigma$ of the muon telescopes. The measurements with the empty target cell have been performed with the central momentum of LEPS reduces by 0.8 MeV/$c$ in order to compensate for the energy loss in the liquid hydrogen. The procedure of background subtraction is visualized and checked in the missing mass spectra. As an example, Fig. 9 displays normalized missing mass spectra for runs with full and empty targets, for both pions and muons. In the different spectra, the peaks due to the scattering on carbon and oxygen cancel to better than 1%. The completeness of the cancellation represents a convincing check of the temporal stability of

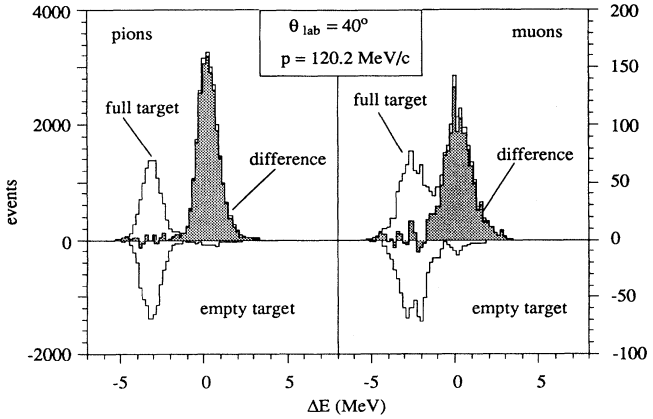


FIG. 9. Energy spectra for pions (left) and muons (right) scattered from the hydrogen target with the target cell alternately full and empty.

the experiment and the correctness of an essential part of the analysis.

### E. Determination of the scattering angle

The smallness of the scattering angles investigated in this experiment requires a precise determination of this quantity. The scattering angle $\psi$ has been calculated from

$$\cos\psi = \frac{\cos\phi_{\rm LEPS} - \sin\phi_{\rm LEPS}\tan\phi_{\rm ST}}{\sqrt{1+\tan^2\phi_{\rm ST}+\tan^2\theta_{\rm ST}}} \tag{10}$$

with $\phi_{\rm LEPS}$ being the angle between the beam axis and the central trajectory of LEPS, and $\phi_{\rm ST}$ and $\theta_{\rm ST}$ the horizontal and vertical angles between the particle trajectory and the central trajectory of LEPS. In this experiment the angles of incidence before scattering have not been measured, in order to avoid having further detector materials in front of the scattering target and to allow the highest possible incident flux. It turns out that the main contribution to the error of the scattering angle was given by the horizontal divergence of the beam, $\sigma_\phi = 2°$, whereas the influence of the vertical divergence could be neglected. In the following the scattering angle calculated with Eq. (10) is denoted by $\theta$.

### F. Evaluation of the cross sections

The data have been analyzed in two essentially independent ways: (A) Absolute differential cross sections for $\pi^\pm p$ scattering have been determined independently for both charges and, (B) ratios of the cross sections for $\pi^+ p$ and $\pi^- p$ scattering (relative numbers) have been derived.

#### *1. Method A*

The determination of the cross sections following the equation

$$\frac{d\sigma}{d\Omega}(\pi^\pm p) = \frac{N_\pi^{\rm scatt}(\theta)}{N_\mu^{\rm scatt}(\theta)}\frac{R_\mu}{R_\pi}\frac{d\sigma}{d\Omega}(\mu^\pm p)\varepsilon \tag{11}$$

requires a knowledge of the electromagnetic cross sections for $\mu^\pm p$ scattering. These have been calculated in the Born approximation (corresponding to one-photon exchange) (all quantities in the center-of-mass system) [33]:

$$\begin{aligned}\frac{d\sigma}{d\Omega}(\mu^\pm p) = {} & \frac{p_\mu^2}{(E_\mu E_p + p_\mu^2)^2 - m_\mu^2 m_p^2}\left(\frac{\alpha}{t}\right)^2 \\ & \times\Bigg\{G_M^2 t[t + E_\mu^2 - p_\mu^2\cos\theta_{\rm c.m.}] \\ & + \left[F_1^2 - \frac{F_2^2 t}{4m_p^2}\right]\left[tm_p^2 + 4(E_\mu E_p + p_\mu^2)\right. \\ & \times\left.\left(E_\mu E_p + p_\mu^2 + \frac{t}{2}\right)\right]\Bigg\}. \end{aligned} \tag{12}$$

The proton form factors are approximated by

$$\begin{aligned} G_E &= \frac{G_M}{2.79} = \left(1 - 0.028\frac{t}{m_\pi^2}\right)^{-2}, \\ F_1 &= \left(G_E - \frac{t}{4m_p^2}G_M\right)\left(1 - \frac{t}{4m_p^2}\right)^{-1}, \\ F_2 &= \frac{G_E - G_M}{t/2m_p - 2m_p}. \end{aligned} \tag{13}$$

Higher-order graphs contribute in the kinematical region under consideration to less than 0.5% and have been neglected.

In the following we describe the corrections to Eq. (11) which are summarized by $\varepsilon = \varepsilon_{\rm conv}\varepsilon_\Omega\varepsilon_{\rm det}$. The various factors represent the corrections for the beam divergence, for the different solid angle of LEPS for pions and muons, and for different detector efficiencies for pions and muons, respectively, as will be discussed below. The corrections for computer dead time and pion decay described in Secs. II D and III C have always been applied but will not be specifically listed below.

During the analysis the angular acceptance of LEPS has been cut to $|\Delta\theta| \le 3°$ and split into angular bins with a width of 1°. The error of the scattering angle is then governed by the horizontal divergence of the incident beam, in the following denoted by $H(\theta)$. The measured cross section, no matter whether $\pi p$ or $\mu p$ scattering is considered, is then given by the "true" cross section convoluted with the divergence of the incident beam:

$$\frac{d\sigma^{\rm exp}}{d\Omega}(\theta) = \int \frac{d\sigma}{d\Omega}(\theta')H(\theta - \theta')d\theta'. \tag{14}$$

The normalized distribution $H(\theta)$ has been determined in a separate experiment where a multiwire proportional chamber with four planes (two for both $x$ and $y$ coordinates) has been installed at the position of the scattering target. By reducing the intensity of the primary proton beam, the complete spatial and angular distribu-

tion $H(x,\theta,y,\phi)$ has been determined under exactly the same experimental conditions as those available during the data-taking runs. By using time-of-flight information, the distributions have been found for pions, muons, and electrons separately. No significant differences have been observed for the distributions for the various particle types and charges. The equality of the pion and muon spatial distributions is a prerequisite for the applicability of our method of normalization of the pion cross sections relative to the electromagnetic ones (with muons and electrons).

In order to calculate the correction arising from the beam divergence,

$$\varepsilon_{\rm conv} = \left(\frac{d\sigma/d\Omega^{\rm exp}(\mu p)}{d\sigma/d\Omega(\mu p)}\right)\left(\frac{d\sigma/d\Omega^{\rm exp}(\pi p)}{d\sigma/d\Omega(\pi p)}\right)^{-1}, \quad (15)$$

the angular distributions for both $\pi p$ and $\mu p$ scattering have to be known. In the case of $\mu p$ scattering, the cross sections have been calculated, as mentioned above, in first order of photon exchange [33]. In the case of $\pi p$ scattering the calculations have been carried out using the phase shifts from the KH80 solution [17]. This procedure is justified since the correction itself, which is plotted in Fig. 10 for pions as a function of the scattering angle, is relatively small and does not exceed 10%.

The efficiency for the detection of pions has been found to be slightly higher than that of muons, resulting in a correction $\varepsilon_{\rm det}$ of the order of 1%. The relative momenta of pions and muons ($\delta_{\pi'}\delta_{\mu}$) scattered from protons differ in their different kinematical energy transfer and energy loss in the target by several percent. This gives rise to a third correction, since the solid angle of LEPS depends on the relative momentum. The resulting correction $\varepsilon_{\Omega} = \Delta\Omega(\delta_{\mu})/\Delta\Omega(\delta_{\pi})$ is precisely known experimentally and never exceeded 5%.

Finally, after calculating the individual cross sections for each angular bin, adjacent bins were systematically combined in pairs to achieve a more transparent presentation and smaller statistical uncertainties relating to the individual points. The results are displayed in Fig. 11 and listed in Tables IV and V.

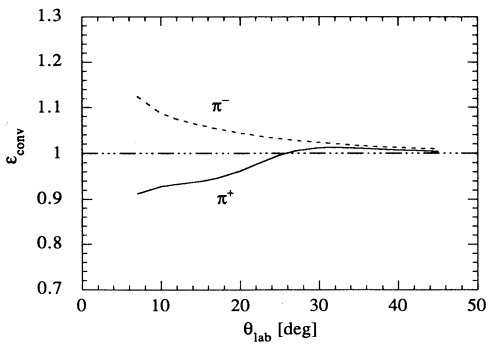


FIG. 10. The correction $\varepsilon_{\rm conv}$, being a consequence of the horizontal divergence of the incident beam, shows a different angular dependence for $\pi^+p$ and $\pi^-p$ scattering.

TABLE IV. Absolutely normalized differential cross sections for $\pi p$ scattering at $T_\pi = 32.2$ MeV.

| $\theta_{\rm c.m.}$ (deg) | $\frac{d\sigma_{\rm c.m.}}{d\Omega}(\pi^+p)$ (mb/sr) | $\frac{d\sigma_{\rm c.m.}}{d\Omega}(\pi^-p)$ (mb/sr) |
|---|---|---|
| 11.77 | 18.013 ± 0.618 | 23.563 ± 0.889 |
| 14.12 | 8.758 ± 0.366 | 12.841 ± 0.406 |
| 16.47 | 4.146 ± 0.180 | 7.340 ± 0.207 |
| 18.81 | 2.543 ± 0.125 | 4.734 ± 0.135 |
| 21.15 | 1.546 ± 0.044 | 3.555 ± 0.087 |
| 23.49 | 0.949 ± 0.029 | 2.528 ± 0.075 |
| 25.82 | 0.672 ± 0.018 | 1.979 ± 0.054 |
| 28.15 | 0.493 ± 0.014 | 1.485 ± 0.061 |
| 30.47 | 0.351 ± 0.010 | 1.321 ± 0.061 |
| 32.78 | 0.262 ± 0.008 | 0.974 ± 0.052 |
| 35.09 | 0.231 ± 0.009 | 0.826 ± 0.054 |
| 37.40 | 0.179 ± 0.006 | 0.792 ± 0.039 |
| 39.69 | 0.172 ± 0.011 | 0.661 ± 0.033 |
| 41.98 | 0.156 ± 0.013 | 0.619 ± 0.030 |
| 44.26 | 0.166 ± 0.016 | 0.548 ± 0.025 |
| 46.53 | 0.167 ± 0.017 | 0.511 ± 0.023 |
| 48.80 | 0.155 ± 0.013 | 0.445 ± 0.021 |
| 51.05 | 0.154 ± 0.009 | 0.429 ± 0.019 |
| 53.30 | 0.194 ± 0.012 | 0.421 ± 0.019 |
| 55.54 | 0.174 ± 0.017 | 0.368 ± 0.023 |

### 2. *Method B*

A second independent analysis which determines only the ratios of the differential cross sections for $\pi^+p$ and $\pi^-p$ scattering has the advantage of smaller systematic uncertainties:

$$\frac{d\sigma/d\Omega(\pi^+p)}{d\sigma/d\Omega(\pi^-p)} = \frac{N^{\rm scatt}_{\pi^+}}{N^{\rm scatt}_{\pi^-}}\frac{N^{\rm in}_{\pi^-}}{N^{\rm in}_{\pi^+}}\varepsilon' . \quad (16)$$

The only correction $\varepsilon'$ which has to be applied is due to contributions arising from the convolution described in

TABLE V. Absolutely normalized differential cross sections for $\pi p$ scattering at $T_\pi = 44.6$ MeV.

| $\theta_{\rm c.m.}$ (deg) | $\frac{d\sigma_{\rm c.m.}}{d\Omega}(\pi^+p)$ (mb/sr) | $\frac{d\sigma_{\rm c.m.}}{d\Omega}(\pi^-p)$ (mb/sr) |
|---|---|---|
| 11.88 | 7.721 ± 0.447 | 13.220 ± 0.722 |
| 14.26 | 3.931 ± 0.262 | 7.749 ± 0.417 |
| 16.62 | 1.681 ± 0.074 | 4.180 ± 0.211 |
| 18.99 | 0.828 ± 0.034 | 2.905 ± 0.164 |
| 21.35 | 0.480 ± 0.019 | 2.307 ± 0.129 |
| 23.70 | 0.250 ± 0.011 | 1.453 ± 0.094 |
| 26.06 | 0.176 ± 0.007 | 1.195 ± 0.058 |
| 28.40 | 0.149 ± 0.007 | 0.961 ± 0.046 |
| 30.74 | 0.109 ± 0.005 | 0.757 ± 0.032 |
| 33.08 | 0.120 ± 0.004 | 0.784 ± 0.031 |
| 35.40 | 0.113 ± 0.004 | 0.590 ± 0.027 |
| 37.72 | 0.132 ± 0.004 | 0.528 ± 0.023 |
| 40.04 | 0.142 ± 0.009 | 0.528 ± 0.043 |
| 42.34 | 0.156 ± 0.015 | 0.524 ± 0.077 |
| 44.64 | 0.160 ± 0.014 | 0.422 ± 0.051 |
| 46.93 | 0.150 ± 0.013 | 0.393 ± 0.056 |
| 49.21 | 0.182 ± 0.018 | 0.410 ± 0.057 |
| 51.47 | 0.212 ± 0.019 | 0.316 ± 0.044 |
| 53.73 | 0.226 ± 0.021 | 0.327 ± 0.038 |
| 55.98 | 0.244 ± 0.031 | 0.342 ± 0.059 |

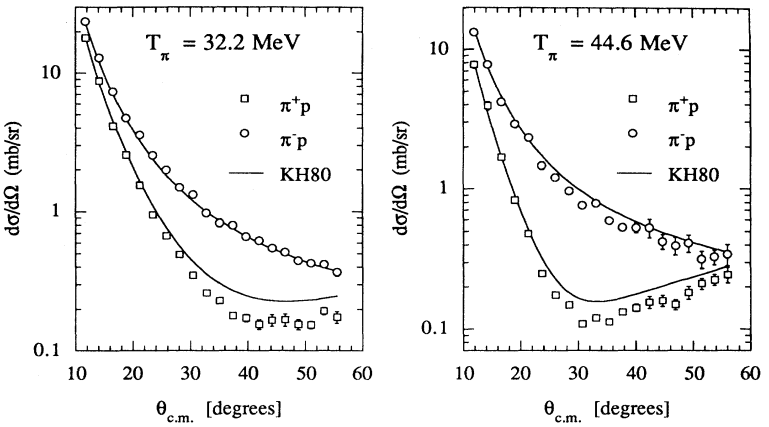


FIG. 11. Differential cross sections for $\pi^+p$ and $\pi^-p$ scattering at $T_\pi$ = 32.2 and 44.6 MeV.

Sec. III F 1 being different for the two particle charges. The efficiencies of particle detection $\varepsilon_{\rm det}$, as well as uncertainties in the solid angle $\varepsilon_\Omega$, factor out completely. The number of incident pions is directly proportional to the counting rate of the muon telescopes, so that, if both runs are again normalized to the same quantity $\mu_\Sigma$, the right side of Eq. (16) reduces to $(N_{\pi^+}^{\rm scatt}/N_{\pi^-}^{\rm scatt})\varepsilon'$. These results combined with the ratios of the cross sections obtained with method A are shown in Fig. 12 and listed in Tables VI and VII. At $T_\pi$ = 44.6 MeV a perfect agreement of the two analyses is found, whereas at $T_\pi$ = 32.2 MeV a systematic deviation of the order of 5% is observed. In order to find an explanation for this deficiency, the ratio of cross sections according to Eq. (16) has been determined for $\mu p$ scattering as well, where for all scattering angles a result very close to unity is expected. In this case the number of incident muons is derived from the counting rate of the muon telescopes by $N_\mu^{\rm in} = \alpha\mu_\Sigma R_\mu/R_\pi$. After normalizing both runs to the same number of counts in the muon telescopes, $\mu_\Sigma$, we obtain

$$\frac{N_{\mu,\rm in}^-}{N_{\mu,\rm in}^+} = \left(\frac{R_\mu}{R_\pi}\right)^- \left(\frac{R_\pi}{R_\mu}\right)^+ . \qquad (17)$$

The results of the analysis for $\mu p$ scattering are shown in Fig. 13. At $T_\pi$ = 44.6 MeV a mean value of 0.995 has been found for the ratio $d\sigma(\mu^+p)/d\sigma(\mu^-p)$, whereas at 32.2 MeV the ratio is 1.044, confirming the deviation mentioned above. We conclude that the two different methods employed to analyze the data are consistent for $T_\pi$ = 44.6 MeV. At 32.2 MeV, however, a systematic error of the order of 5% remains, the origin of which must be found in the normalization procedure with muon scattering.

### 3. *Discussion of the results and comparison with the KH80 phase shift analysis*

The angular distributions shown in Figs. 11 and 12 are dominated by the steep slope at small scattering angles which is typical of the electromagnetic interaction. The interference of the electromagnetic and the strong interaction being destructive for $\pi^+p$ and constructive for $\pi^-p$ scattering leads to a pronounced minimum in the first case at center-of-mass angles around 30° to 40°. A comparison with the prediction of the Karlsruhe-Helsinki phase shift analysis KH80, which forms the basis for the current experimental value of the $\sigma_{\pi N}$ term, reveals discrepancies which are most pronounced for $\pi^+p$ scattering at the largest angles measured in this experiment. At the smallest scattering angles, however, i.e., in the Coulomb interference dominated region, the experimental values are in excellent agreement with the predictions for both charges and both energies. This is a stringent test of the

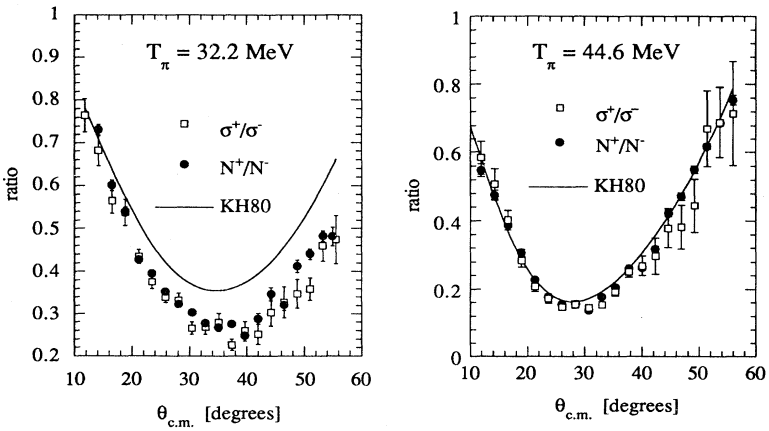


FIG. 12. Ratio of the differential cross sections for $\pi^+p$ and $\pi^-p$ scattering in comparison with that of the counting rates $N^+/N^-$ (see the text for details).

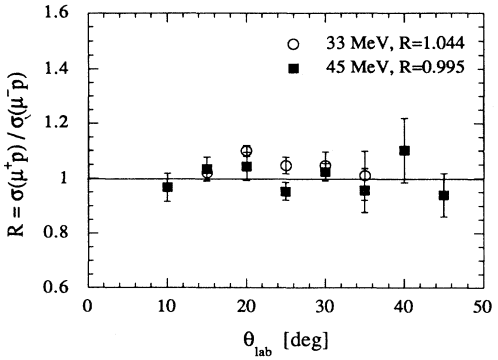


FIG. 13. Measured ratios of cross sections for $\mu^+p$ and $\mu^-p$ scattering.

normalization method applied to the data. A deviation from the calculated values in this region would clearly hint at systematic errors in the normalization. At scattering angles larger than 20° the $\pi^+p$ data collected at both energies are significantly lower than the KH80 prediction. For the $T_\pi = 32.2$ MeV data, the discrepancy reaches a value of about 0.07 mb/sr at $\theta_{\text{c.m.}} \approx 40°$, being constant thereafter up to the largest measured angle. In the case of the 44.6 MeV data, a constant discrepancy of about 0.04 mb/sr is observed for angles larger than $\theta_{\text{c.m.}} \approx 30°$. This corresponds to relative deviations of about −30% and −20% at 32.2 and 44.6 MeV, respectively. The $\pi^-p$ cross sections at 32.2 MeV are marginally higher than the KH80 predictions, whereas at 44.6 MeV the experimental values are below the predictions by up to about 15% at angles from 20° on. A comparison of the ratios of $\pi^+p/\pi^-p$ cross sections with the phase shift prediction gives different results for the two energies (see Fig. 12). At 32.2 MeV the ratios obtained with both methods (A) and (B) lie considerably below the KH80 prediction. At 44.6 MeV, where deviations of the measured cross sections from the KH80 solution have been observed for $\pi^+p$ as well as for $\pi^-p$ scattering, the ratio of the cross sections is in reasonable agreement with the KH80 prediction.

TABLE VI. Ratios of differential cross sections for $\pi^+p$ and $\pi^-p$ scattering at $T_\pi = 32.2$ MeV.

| $\theta_{\text{c.m.}}$ (deg) | $N^+_{\text{scatt}}/N^-_{\text{scatt}}$ | $\sigma_{\pi^+}/\sigma_{\pi^-}$ |
|---|---|---|
| 11.77 | | 0.765 ± 0.039 |
| 14.12 | 0.731 ± 0.012 | 0.682 ± 0.036 |
| 16.47 | 0.601 ± 0.012 | 0.565 ± 0.029 |
| 18.81 | 0.539 ± 0.011 | 0.537 ± 0.031 |
| 21.15 | 0.428 ± 0.007 | 0.435 ± 0.016 |
| 23.49 | 0.395 ± 0.007 | 0.375 ± 0.016 |
| 25.82 | 0.352 ± 0.005 | 0.339 ± 0.013 |
| 28.15 | 0.323 ± 0.007 | 0.332 ± 0.017 |
| 30.47 | 0.303 ± 0.006 | 0.266 ± 0.014 |
| 32.78 | 0.278 ± 0.006 | 0.269 ± 0.016 |
| 35.09 | 0.267 ± 0.007 | 0.279 ± 0.021 |
| 37.40 | 0.276 ± 0.007 | 0.226 ± 0.014 |
| 39.69 | 0.249 ± 0.013 | 0.260 ± 0.021 |
| 41.98 | 0.288 ± 0.013 | 0.251 ± 0.024 |
| 44.26 | 0.347 ± 0.016 | 0.303 ± 0.032 |
| 46.53 | 0.321 ± 0.013 | 0.328 ± 0.037 |
| 48.80 | 0.412 ± 0.015 | 0.348 ± 0.034 |
| 51.05 | 0.441 ± 0.013 | 0.359 ± 0.027 |
| 53.30 | 0.483 ± 0.012 | 0.460 ± 0.036 |
| 55.54 | 0.482 ± 0.022 | 0.474 ± 0.056 |

TABLE VII. Ratios of differential cross sections for $\pi^+p$ and $\pi^-p$ scattering at $T_\pi = 44.6$ MeV.

| $\theta_{\text{c.m.}}$ (deg) | $N^+_{\text{scatt}}/N^-_{\text{scatt}}$ | $\sigma_{\pi^+}/\sigma_{\pi^-}$ |
|---|---|---|
| 10.10 | 0.653 ± 0.025 | |
| 11.88 | 0.548 ± 0.019 | 0.584 ± 0.046 |
| 14.26 | 0.475 ± 0.015 | 0.507 ± 0.043 |
| 16.62 | 0.386 ± 0.012 | 0.402 ± 0.027 |
| 18.99 | 0.308 ± 0.010 | 0.285 ± 0.020 |
| 21.35 | 0.228 ± 0.006 | 0.208 ± 0.014 |
| 23.70 | 0.177 ± 0.006 | 0.172 ± 0.013 |
| 26.06 | 0.155 ± 0.004 | 0.147 ± 0.009 |
| 28.40 | 0.156 ± 0.004 | 0.155 ± 0.010 |
| 30.74 | 0.136 ± 0.003 | 0.144 ± 0.009 |
| 33.08 | 0.178 ± 0.003 | 0.153 ± 0.008 |
| 35.40 | 0.205 ± 0.003 | 0.192 ± 0.011 |
| 37.72 | 0.260 ± 0.003 | 0.250 ± 0.013 |
| 40.04 | 0.262 ± 0.005 | 0.269 ± 0.028 |
| 42.34 | 0.317 ± 0.009 | 0.298 ± 0.052 |
| 44.64 | 0.421 ± 0.010 | 0.379 ± 0.057 |
| 46.93 | 0.471 ± 0.012 | 0.382 ± 0.064 |
| 49.21 | 0.550 ± 0.011 | 0.444 ± 0.076 |
| 51.47 | 0.617 ± 0.009 | 0.671 ± 0.111 |
| 53.73 | 0.687 ± 0.009 | 0.691 ± 0.103 |
| 55.98 | 0.754 ± 0.014 | 0.713 ± 0.153 |

### G. Discussion of errors

In addition to the standard deviation representing the pure statistical errors deduced from the number of scattering events, the errors quoted in Tables IV–VII include contributions from two other sources: The error resulting from the cuts discussed in Sec. III C applied in order to select scattered pions or muons, and the uncertainty originating from the muonic background remaining in the pionic spectra after applying all cuts. While the first contribution has been estimated to be less than 1.8% by systematic variation of the cuts, the latter uncertainty has been calculated by means of simulations with the computer code DECAY TURTLE [31] to be smaller than 0.5%. Since the cuts have been determined for each data point separably, the errors have been added quadratically to the standard deviation.

In the following we discuss the various systematic errors which have been added linearly in order to arrive at a maximum error in the absolute normalization. The uncertainty of the identification of the incident particles represents an essential contribution to the error of the normalization. By varying the cuts in the TOF spectra (see Sec. III B) this contribution, which does not depend on the scattering angle, has been found to be less than ±2%. Since the electromagnetic cross sections for $\mu^\pm p$ scattering exhibit a strong energy dependence, the ab-

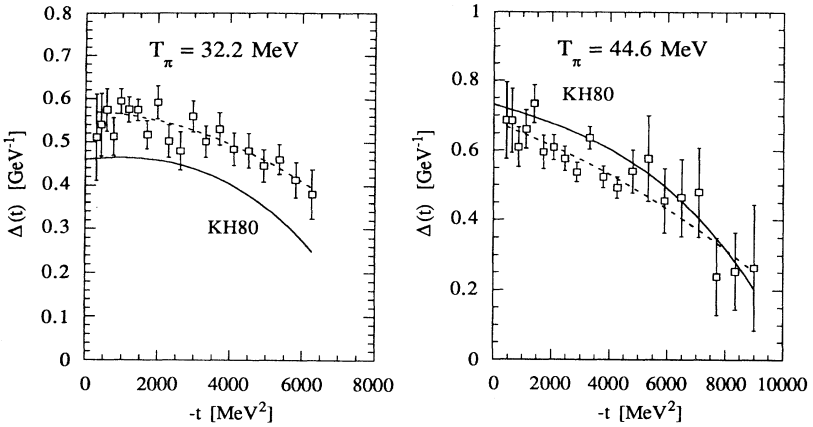


FIG. 14. The difference of the cross sections of $\pi^+p$ and $\pi^-p$ scattering divided by $4\,\mathrm{Re}G_C(t)$. The solid line marks the prediction of the KH80 phase shift analysis, whereas the dashed line corresponds to a fit to the data with a polynomial of second order in $t$.

solute normalization of the $\pi^{\pm}p$ data suffers from the limited accuracy with which the energy of the incident muons is known. The resulting uncertainty has been calculated to be about $\pm 0.8\%$ and turns out to be more or less independent of the scattering angle. Due to the mechanical tolerances in the alignment of the wire chamber in the intermediate focus of LEPS, the central horizontal scattering angle is known to within an error of only 2 mrad and is identical for pions and muons. At small scattering angles, where the pion and muon cross sections show a very similar angular dependence, the resulting uncertainties are negligible. For larger angles, however, uncertainties up to $\pm 2.5\%$ can be introduced by this effect. Two minor uncertainties originate from the correction terms $\varepsilon_{\mathrm{conv}}$ and $\varepsilon_{\Omega}$ discussed in Sec. III F 1. By systematically varying the angular resolution determining $\varepsilon_{\mathrm{conv}}$, an uncertainty below $\pm 1\%$ has been found. The error introduced by the correction $\varepsilon_{\Omega}$, the values of which are of the order of $\pm 5\%$, is believed to be negligible. We conclude that the maximum uncertainty of the absolute normalization of the $\pi^{\pm}p$ cross sections at 32.2 and 44.6 MeV is $\pm 6.3\%$. If we sum up the individual contributions quadratically, a method sometimes favored by other authors, we obtain $\pm 3.4\%$.

In the case of ratios of the cross sections described in Sec. III F 2, both the statistical and systematic errors are smaller than for the individual cross sections. On the one hand, this is due to the higher counting statistics for pions compared to that for muons. On the other hand, some of the systematic uncertainties factor out in the ratio, resulting in a maximum error for the absolute normalization of $\pm 3.5\%$.

### H. Determination of $\mathrm{Re}D^+(t=0)$

As outlined in the Introduction, an experiment measuring both $\pi^+p$ and $\pi^-p$ scattering in the region of the Coulomb nuclear interference allows a direct determination of the isospin-even forward scattering amplitude $\mathrm{Re}D^+(t=0)$ at vanishing four-momentum transfer $t$ [Eq. (3)]. The expression for $\Delta(t)$ is shown in Fig. 14 for $T_\pi = 32.2$ and 44.6 MeV. A polynomial of second order in $t$, $f(t) = c_0 + c_1 t + c_2 t^2$, has been fitted to the data, where the coefficient $c_0$ determines $\Delta(t=0)$. A second approach, employing only the ratios of the $\pi^+p$ and $\pi^-p$ cross sections,

$$\mathrm{Re}D^+(t=0) = \frac{4\pi\sqrt{s}}{m_N} \lim_{t\to 0} \frac{\sigma(\pi^+p)/\sigma(\pi^-p) - 1}{\sigma(\pi^+p)/\sigma(\pi^-p) + 1} \times \frac{|G_C(t)|^2}{2\,\mathrm{Re}G_C(t)} \tag{18}$$

should in principle be more precise, since some of the errors discussed in Sec. III G factor out. These advantageous factorings out are, however, detracted from by the uncertainties associated with the more complicated $t$ dependence of Eq. (18), which is in turn well described by a function such as

$$f(t) = c_1 \frac{1 + c_2 t + c_3 t^2}{1 + c_4 t + c_5 t^2}\,. \tag{19}$$

In order to minimize the uncertainties resulting from the extrapolation to $t = 0$, all coefficients have been given initial values by fitting them to the predictions of the KH80 phase shift analysis. Subsequently only the coefficients $c_1$ and $c_3$ representing $\mathrm{Re}D^+(t=0)$ and the curvature of $\mathrm{Re}D^+$ have been freely determined. Instead of calculating the ratios $\sigma(\pi^+p)/\sigma(\pi^-p)$ from the individually determined cross sections (see Sec. III F 1), the ratios (see Sec. III F 2) have been used in a third variant to evaluate $\mathrm{Re}D^+(t=0)$. A final approach makes use of the direct and separate determination of the forward scattering amplitudes for $\pi^+p$ and $\pi^-p$ scattering:

$$\mathrm{Re}D_{\pm}(t=0) = \lim_{t\to 0} \left( \frac{4\pi\sqrt{s}}{m_N} \frac{d\sigma(\pi^{\pm}p)/d\Omega - |G_C(t)|^2}{2\,\mathrm{Re}G_C(t)} \right). \tag{20}$$

Subsequently the isospin-even amplitude can be calculated by averaging the amplitudes for $\pi^+p$ and $\pi^-p$ scattering through

$$\mathrm{Re}D^+(t=0) = \tfrac{1}{2}\mathrm{Re}[D_+(t=0) + D_-(t=0)]\,.$$

A summary of the results of the four approaches and a comparison with the predictions of the KH80 phase shift

TABLE VIII. Results of the various methods used to determine $\mathrm{Re}D^+(t=0)$.

| $\mathrm{Re}D^+(t=0)$ ($\mathrm{GeV}^{-1}$) | 32.2 MeV | 44.6 MeV |
|---|---|---|
| $\sigma^+ - \sigma^-$ | $8.4 \pm 0.3$ | $10.2 \pm 0.5$ |
| $\sigma^+/\sigma^-$ | $8.2 \pm 0.5$ | $11.3 \pm 1.0$ |
| $N^+/N^-$ | $8.0 \pm 0.5$ | $11.3 \pm 1.0$ |
| $\frac{1}{2}(D_+ + D_-)$ | $8.2 \pm 0.7$ | $10.3 \pm 0.8$ |
| Weighted mean | $8.2 \pm 0.3$ | $10.5 \pm 0.5$ |
| KH80 | 6.8 | 10.9 |

analysis is given in Table VIII.

The four different approaches lead to results for $\mathrm{Re}D^+(t=0)$ which are consistent within the quoted uncertainties. The uncertainties in the weighted means, incorporating the results stemming from each of the four methods, have been associated, in a conservative way, with the errors of the first method. Since the different results are based on the same experimental input, a conventional propagation of the errors would produce estimates too optimistic for those of the weighted means.

At $T_\pi = 32.2$ MeV the comparison with the prediction of the KH80 phase shift solution for the nuclear amplitude $\mathrm{Re}D^+(t=0)$ reveals a considerable discrepancy, whereas at 44.6 MeV the experimental value is still compatible with the predicted one. In Fig. 15 $\mathrm{Re}D^+(t=0)$ is plotted versus the center-of-mass momentum squared. The choice of the abscissa is motivated by the usual low-energy expansion of the partial waves at threshold (effective range approximation), $f_l = q^{2l}(a_l + q^2 b_l + \cdots)$ with $l$ specifying the angular momentum. Even if the effective range approximation is valid only up to $T_\pi \approx 30$ MeV a smooth and only weakly curved behavior of $\mathrm{Re}D^+(t=0)$ is expected in our energy range. Figure 15 includes two further points from an earlier experiment at $T_\pi = 54.3$ MeV [23,24]. Generally speaking, the experimentally determined values of $\mathrm{Re}D^+(t=0)$ confirm the $q$ dependence of the KH80 prediction and point to an even higher value at the lowest energy.

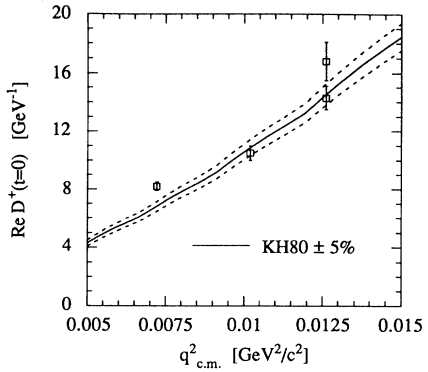


FIG. 15. The real part of the isospin-even amplitude $D^+(t=0)$ plotted versus the center-of-mass momentum squared. Two values are included at $q^2 = 0.0126$ $\mathrm{GeV}^2/c^2$ from Refs. [23,24]. The solid line corresponds to the prediction of the KH80 phase shift solution. The error band of $\pm 5\%$ has been chosen in accordance with the errors of the $S$-wave scattering lengths, as given by Koch in his analysis of low-energy pion nucleon scattering [34].

## IV. SUMMARY

In this article the experimental determination of the differential cross sections of pion proton scattering at pion kinetic energies $T_\pi = 32.2$ and 44.6 MeV has been described. The angular region ($10^\circ \leq \theta_{\mathrm{lab}} \leq 45^\circ$) comprises the region of the Coulomb nuclear interference and hence allows the direct evaluation of the real part of the isospin-even pion nucleon amplitude $\mathrm{Re}D^+(t=0)$. The experimental method, especially the use of high-resolution magnet spectrometer equipped with various wire chambers and scintillation detectors, allows the collection of data with the large amount of redundancy which is indispensable for a reliable analysis. As a consequence, the analysis is almost completely free of Monte Carlo corrections which often induce additional uncertainties. The measured cross sections have been compared with the predictions of the phase shift analysis KH80, revealing discrepancies mainly for the $\pi^+ p$ data which amount to about 30% at 32.2 MeV. The numbers for $\mathrm{Re}D^+(t=0)$, however, substantiate the high value for the $\Sigma$ amplitude at the Cheng-Dashen point. Although a final conclusion concerning the value of this amplitude can be drawn only after a new dispersion analysis, which has to incorporate the complete pion nucleon database, the discrepancy between the experimental $\sigma$ term and the value obtained from the baryonic mass spectrum seems to persist. The question of the contribution of $\bar{s}s$ sea quark pairs to the mass of the nucleon still awaits conclusive resolution.

## ACKNOWLEDGMENTS

We are very grateful to Professor G. Höhler who introduced us into the field of pion nucleon interactions, continuously encouraged our work, and followed our results with great interest. We thank K. Kärcher for very competent technical assistance. The excellent cooperation of our PSI/SIN colleagues and the hospitality we have encountered at PSI are greatly appreciated. This work was supported by the German Federal Ministry of Research and Technology (Bundesministerium für Forschung und Technologie) under Contracts No. 06-KA-266, No. 06-KA-654 I TP3, No. 06-TÜ-243, and No. 06-TÜ-656.

[1] R. L. Jaffe, Nucl. Phys. **A478**, 3c (1988).

[2] J. Gasser and H. Leutwyler, Phys. Rep. C **87**, 77 (1982); Phys. Lett. **125B**, 321 (1983); **125B**, 325 (1983); Ann. Phys. (N.Y.) **158**, 142 (1984); Nucl. Phys. **B250**, 465 (1985); **B250**, 517 (1985); **B250**, 539 (1985).

[3] J. Gasser, in *Proceedings of the International Conference on a European Hadron Facility*, Mainz, 1986, edited by Th. Walcher [Nucl. Phys. **B279**, 65 (1987)]; in Pro-

ceedings of the Second International Workshop on $\pi N$ Physics, LAMPF, 1987, edited by W. R. Gibbs and B. M. K. Nefkens (LAMPF Report No. LA-11184-C, 1987), p. 266.

[4] J. Gasser, H. Leutwyler, and M. E. Sainio, Phys. Lett. B **253**, 252 (1991); **253**, 260 (1991).

[5] J. Gasser, H. Leutwyler, M. P. Locher, and M. E. Sainio, Phys. Lett. B **213**, 85 (1988).

[6] J. Gasser, M. E. Sainio, and A. Svarc, Nucl. Phys. **B307**, 779 (1988).

[7] J. Ashman *et al.*, Nucl. Phys. **B328**, 1 (1989).

[8] R. Decker, Th. Leize, and M. Nowakowski, Phys. Lett. B **244**, 497 (1990).

[9] H. Fritzsch, Phys. Lett. B **256**, 75 (1991).

[10] D. Kaplan and A. Manohar, Nucl. Phys. **B310**, 527 (1988).

[11] R. McKeown *et al.*, Proposal to the MIT–Bates Linac Center, 1989.

[12] R. Decker, M. Nowakowski, and J. Stahov, Nucl. Phys. **A512**, 626 (1990).

[13] R. Decker and Th. Leize, Phys. Lett. B **246**, 233 (1990).

[14] R. Decker, Th. Leize, and M. Nowakowski, Z. Phys. C **50**, 305 (1991).

[15] B. R. Holstein, Phys. Lett. B **244**, 83 (1990).

[16] E. Pietarinen, Nucl. Phys. **B107**, 21 (1976); G. Höhler, F. Kaiser, R. Koch, and E. Pietarinen, *Handbook of Pion-Nucleon Scattering*, Physics Data Vol. 12-1 (Fachinformationszentrum, Energie, Physik, Mathematik, Karlsruhe, 1979); R. Koch, Z. Phys. C **15**, 161 (1982); G. Höhler, in *Methods and Results of Phenomenological Analyses*, edited by H. Schopper, Landolt-Börnstein, New Series, Group 1, Vol. 9, Part b2 (Springer-Verlag, Berlin, 1983).

[17] R. Koch and E. Pietarinen, Nucl. Phys. **A336**, 331 (1980).

[18] E. G. Auld *et al.*, Can. J. Phys. **57**, 73 (1979); B. G. Ritchie, R. S. Moore, B. M. Preedom, G. Das, R. C. Minehart, K. Gotow, W. J. Burger, and H. J. Ziock, Phys. Lett. **125B**, 128 (1983); J. S. Frank, A. A. Browman, P. A. M. Gram, R. H. Heffner, K. A. Klare, R. E. Mischke, D. C. Moir, D. E. Nagle, J. M. Potter, R. P. Redwine, and M. A. Yates, Phys. Rev. D **28**, 1569 (1983); J. T. Brack *et al.*, Phys. Rev. C **34**, 1771 (1986); **38**, 2427 (1988); **41**, 2202 (1990); P. Y. Bertin, B. Coupat, A. Hivernat, D. B. Isabelle, J. Duclos, A. Gerard, J. Miller, J. Morgenstern, J. Picard, P. Vernin, and R. Powers, Nucl. Phys. **B106**, 341 (1976).

[19] W. Kluge, in *Pion-Nucleus Physics: Future Directions and New Facilities at LAMPF*, edited by R. J. Peterson and D. D. Strottman, AIP Conf. Proc. No. 163 (AIP, New York, 1988), p. 247; in *Proceedings of the Third International Symposium on Pion-Nucleon and Nucleon-Nucleon Physics*, Gatchina/Leningrad, 1989, edited by S. P. Kruglov and J. W. Lopatin (Academy of Sciences of the USSR, Leningrad Nuclear Physics Institute, Leningrad, 1989), Vol. I, p. 193; in *Proceedings of the International Conference on Mesons and Nuclei at Intermediate Energies*, Dubna, 1994, edited by M. Khankhasayev (World Scientific, Singapore, in press); in *Proceedings of the International Conference on Physics with GeV-Particle Beams*, Jülich, 1994, edited by K. Kilian, J. Speth, and T. Mayer-Kuckuk (World Scientific, Singapore, in press).

[20] Ch. Joram, in Proceedings of the IV International Symposium on Pion-Nucleon Physics and the Structure of the Nucleon, Bad Honnef, 1991, edited by G. Höhler, W. Kluge, and B. M. K. Nefkens ($\pi N$ Newsletter No. 5 1992), p. 117; in Proceedings of the V International Symposium on Meson Nucleon Physics and the Structure of the Nucleon, Boulder, CO, 1993, edited by G. Höhler, W. Kluge, and B. M. K. Nefkens ($\pi N$ Newsletter No. 8, 1993), p. 30.

[21] G. Höhler, in $\pi N$ Newsletter No. 2, 1990, University of Karlsruhe and University of California Los Angeles, edited by G. Höhler, W. Kluge, and B. M. K. Nefkens, p. 1; G. Höhler and J. Stahov, *ibid.* p. 42; G. Höhler, Nucl. Phys. **A508**, 525c (1990).

[22] E. Friedman, in Proceedings of the IV International Symposium on Pion Nucleon Physics and the Structure of the Nucleon, Bad Honnef, 1991, edited by R. Decker, G. Höhler, M. G. Huber, and W. Kluge ($\pi N$ Newsletter No. 4, 1991), p. 1.

[23] U. Wiedner, K. Göring, J. Jaki, U. Klein, W. Kluge, H. Matthäy, M. Metzler, E. Pedroni, W. Fetscher, H. J. Gerber, and R. Koch, Phys. Rev. Lett. **58**, 648 (1987); Phys. Rev. D **40**, 3568 (1989).

[24] U. Wiedner, Ph.D. thesis, University of Karlsruhe (Report Kfk No. 4317, Karlsruhe, 1987).

[25] M. Metzler, Ph.D. thesis, University of Karlsruhe, 1990 (unpublished); M. Metzler, B. M. Barnett, R. Bilger, H. Clement, J. Jaki, Ch. Joram, K. Kärcher, Th. Kirchner, W. Kluge, S. Krell, H. Matthäy, G. J. Wagner, and R. Wieser, in $\pi N$ Newsletter No. 2, 1990, edited by G. Höhler, W. Kluge, and B. M. K. Nefkens, p. 32.

[26] Ch. Joram, B. M. Barnett, R. Bilger, H. Clement, J. Jaki, K. Kärcher, Th. Kirchner, W. Kluge, S. Krell, H. Matthäy, M. Metzler, G. J. Wagner, and R. Wieser, in $\pi N$ Newsletter No. 2 [25], p. 39.

[27] H. Matthäy, K. Göring, J. Jaki, W. Kluge, M. Metzler, and U. Wiedner, in *Proceedings of the International Symposium on Dynamics of Collective Phenomena in Nuclear and Subnuclear Long Range Interactions in Nuclei*, Bad Honnef, 1987, edited by P. David (World Scientific, Singapore, 1988).

[28] H. Matthäy and W. Kluge, SIN Jahresbericht 1982, p. JB 23; SIN Jahresbericht 1984, p. JB 25; SIN Jahresbericht 1986, p. JB 16.

[29] B. M. Barnett, S. Krell, H. Clement, G. J. Wagner, J. Jaki, Ch. Joram, W. Kluge, H. Matthäy, and M. Metzler, Nucl. Instrum. Methods Phys. Res. Sect. A **297**, 444 (1990).

[30] R. Langley, Nucl. Instrum. Methods **113**, 109 (1973); K. W. Kemper and J. D. Fox, *ibid.* **105**, 333 (1972); M. Martini, T. W. Raudorf, W. R. Stott, and J. C. Waddington, IEEE Trans. Nucl. Sci. **NS22**, 145 (1975); M. Ogihara, Y. Nagashima, W. Galster, and T. Mikumo, Nucl. Instrum. Methods Phys. Res. Sect. A **251**, 313 (1986).

[31] K. L. Brown and Ch. Iselin, "DECAY TURTLE," Report No. CERN-80-04, 1980.

[32] Ch. Joram, Diploma thesis, University of Karlsruhe, 1989 (unpublished).

[33] H. M. Pilkuhn, *Relativistic Particle Physics* (Springer-Verlag, New York, 1979).

[34] R. Koch, "Inconsistencies in Low-Energy Pion Nucleon Scattering," Karlsruhe Report No. TKP 85-5, 1985.